TD-03-019
May 03

Fermi National Accelerator Laboratory
Technical Division / Development & Test Dept.
PO Box 500 MS 316
Batavia, IL 60510
FAX : 630-840-2383

Measurements and Modeling of Thermal Conductivity of Impregnated Nb_3Sn Cable Stacks

L. Imbasciati, G. Ambrosio, P. Bauer,
Fermilab – Technical Division / Test and Development Department
D. Pedrini, V. Previtali, L. Rossi, G. Volpini
University of Milan and INFN-LASA

Abstract:

Nb_3Sn is, at present, the best superconductor for high field accelerator magnets. Several models using Nb_3Sn are under development in many laboratories. Knowledge of the thermal properties of the impregnated coils is of crucial importance for the design of these magnets. In fact, the performance of epoxy-impregnated coils is sensitive to the thermal conductivity value, especially in case of heating caused by hysteretic losses, which are usually relevant in Nb_3Sn magnets, and in the case of continuous heat deposition, such as in magnets near the interaction region of a collider. Different insulation materials have been studied at Fermilab utilizing various design approaches and fabrication methods. Thermal conductivity measurements, at cryogenic temperatures, have been performed at INFN-LASA in collaboration with Fermilab. The measurement data are reported in this note and compared with calculation results from thermal conductivity models of the cable stacks.

1. Thermal conductivity measurements of cable stacks

The knowledge of the thermal properties of the impregnated coils is of crucial importance for the design of Nb_3Sn magnets. In fact, the performance of epoxy-impregnated coils, which are cooled indirectly, is sensitive to the value of the thermal conductivity. This is particularly true in the case of heating caused by hysteretic losses, which are usually relevant in Nb_3Sn magnets because of their large effective filament diameter, and in the case of continuous heat deposition, such as in magnets near the interaction regions of a collider [1]. Although the thermal properties of the individual materials forming the coils are well known, the resulting overall properties can hardly be predicted with a good accuracy. The thermal conductivity at cryogenic temperature of impregnated Nb_3Sn cable stacks with different insulations was measured at the INFN Laboratory for Applied Superconductivity and Accelerators (LASA) in Milan (Italy), and in collaboration with the University of Milan.

1.1 Experiment Description

1.1.a Description of the samples

The samples are stacks of reacted Rutherford cables, vacuum impregnated with epoxy resin (CTD-101K [2]) under a pressure of 15 MPa. The sample characteristics are listed in Table 1. The first sample is a 13 cables-stack, 86 mm long. All the other samples are ten-stacks, 25.4 mm long.

The cables are insulated with some of the different materials under study at Fermilab in the frame of the Nb_3Sn magnet program. An insulation scheme based on ceramic-fiber tape with ceramic binder [3] is a key element of the production of the FNAL cos-theta dipole. E-glass, Kapton® and pre-impregnated fiberglass (pre-preg) tapes [4] have been studied during the R&D for FNAL single-layer common coil and racetrack magnets.

Sample#		1	2	3	4 & 5
Insulation material		Fiberglass (E-glass)	Kapton+ Pre-preg	Only epoxy	Ceramic fibers + binder
Ins. thickness	(mm)	0.2	0.23	-	0.35
Strand diameter	(mm)	0.7	0.7	0.7	1
Cu/non-Cu		1.4	0.87	0.87	0.92
Packing factor		0.87	0.87	0.87	0.9
Cable thickness	(mm)	1.2	1.2	1.2	1.8
Cable width	(mm)	14.5	14.5	14.5	14

Table 1: Main parameters of cable stacks for the conductivity measurements.

The first three samples are stacks of cables with the same design (41 strands of 0.7 mm diameter). Similar cables were used for the construction of two racetrack magnets at Fermilab [5]. In the first sample, a fiberglass tape is wrapped around each cable with 30% overlap. In the second sample, the turn-to-turn insulation consists of a layer of Kapton® -thick), and a layer of pre-impregnated fiberglass tape. The final average thickness of the insulating layer, after impregnation, is 0.23 mm. The third sample is a stack of the same cable as in sample # 2, but it is epoxy-impregnated without any other insulating material. In this sample, the cables are in direct thermal contact. Therefore, the measure of the thermal conductivity of this sample, allowed the direct measure of the impregnated cable, and the contribution of the insulating layer to the overall coil thermal conductivity.

The last two samples in Table 1 are ten-stacks of a cable with 28 strands, 1 mm in diameter, as the cable used in the Fermilab cos-theta dipole magnets. This cable has a higher compaction and higher copper content than the cable of samples # 2 and # 3. Samples # 4 and # 5, are prepared following the same procedure used for the production of the coils of the cos-theta dipole models. Each cable is wrapped with ceramic fibers tape, with 40 % overlap, then is wetted with a ceramic binder (CTD-1002x), and cured at 80 °C for 20 minutes. The samples are then heat treated to form the Nb_3Sn composite. Analysis at the SEM show that, after the heat treatment, the cable strands are coated with a thin layer of a material with a high content of oxygen and silica [6]. The effect of this coating on the contact electrical resistance between the strands is under investigation at Fermilab [7].

1.1.b Apparatus description

The experimental setup, described in detail in [8] is briefly presented here. The conductivity measurement was performed using a steady-state method, described in the following: the sample is placed between two heat sinks, providing a constant heat flux in one (axial) dimension, when thermal equilibrium is reached. The cold sink is in direct contact with the cryogen, and the warm sink is heated through an electrical resistance. The measures of the current and of the voltage across the resistor provide a precise value of the input power. The heat flux is then given by the power divided by the area of the cross section of the sample. The temperature is measured at several points along the sample and on the two sinks, through Au-Fe (0.07 % at w.) – Chromel-P thermo-couples. The system is enclosed in a vacuum chamber in which the pressure is maintained at about 10^{-6} mbar, to avoid convective losses. The vacuum chamber is made of stainless steel, and is gold plated to reduce radiative losses. The main parts of the apparatus are shown in Fig. 4.

The Fourier-Biot law determines the thermal conductivity:

$$\dot{Q} = -k \cdot S \cdot dT/dl \quad (\mathrm{W}) \tag{1}$$

where $\dot{Q} = -P$ is the heat flowing in the sample (equal to the input power P, but in opposite direction with respect to the temperature differential dT/dl); k is the thermal conductivity (which is temperature dependent); and S is the cross-sectional area of the sample. Considering S a constant, and approximating k to be a linear function of temperature, we can calculate the thermal conductivity at an average temperature $\overline{T} = (T_1 + T_2)/2$, with $\Delta T = T_1 - T_2$, using (2):

$$k(\overline{T}) = P \cdot l/(S \cdot \Delta T) \quad \left(\frac{\mathrm{W}}{\mathrm{K} \cdot \mathrm{m}}\right). \tag{2}$$

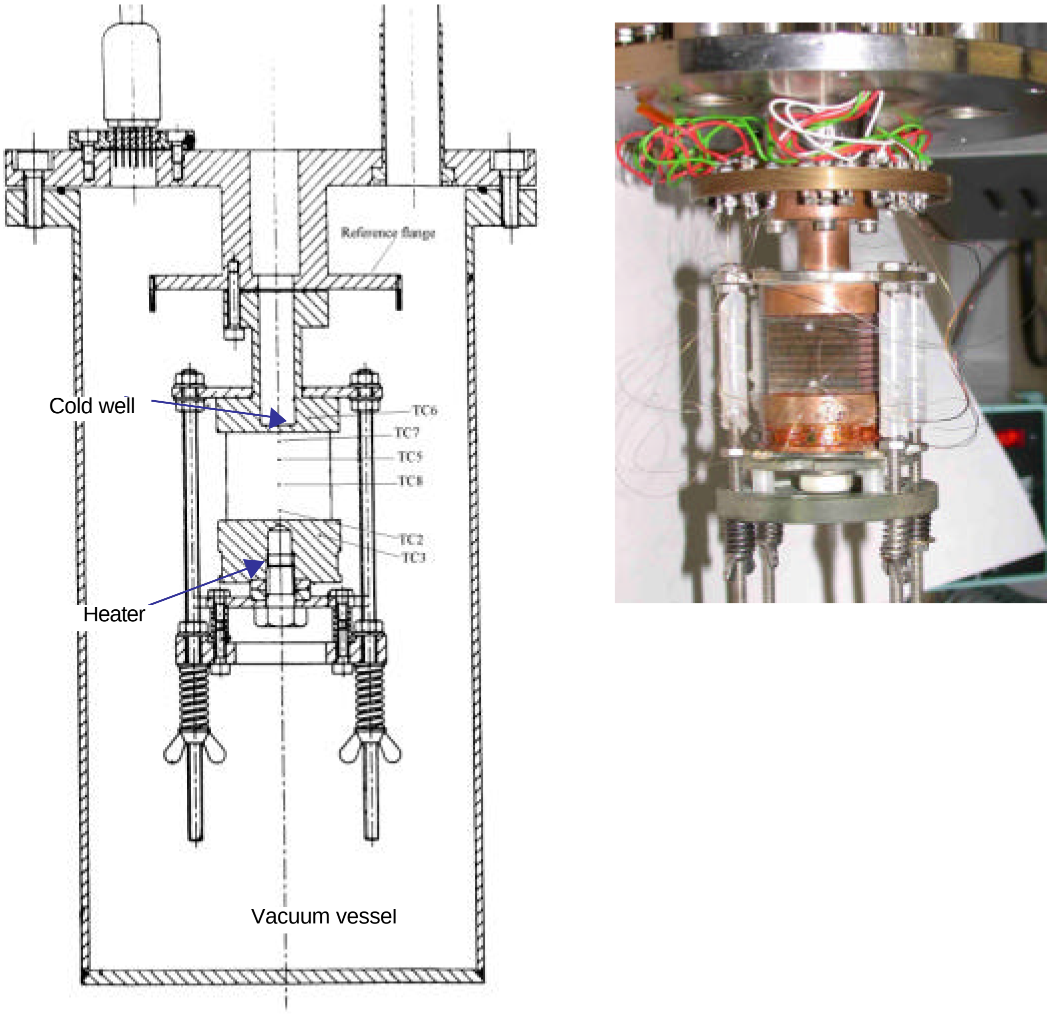

Fig. 1: Schematic drawing of the conductivity measurement and sample holder.

The approximation of $k(T)$ as a linear function is a good approximation for metals at low temperature, or if the conductivity dependence on temperature is a slowly varying function. The conductivity of the insulating materials typically has a steep increase at low temperature. In the case of our composite samples, at temperatures close to liquid Helium temperature, the error due to this approximation is small for temperature differences of a few Kelvin (Fig. 2).

Another source of error is the power loss, due to heat dissipated by convection through the supporting system, convective losses through residual gas, and radiation from the warm sample and from the heater to the vacuum vessel at bath temperature. The setup is designed and tested to have very low power losses, estimated to be about 3 % of the input power, in most of the temperature range of operation with liquid Helium [8]. A maximum dissipation of 10 % is possible using liquid nitrogen, due to larger temperature differences.

2. Experimental results

Fig. 2 shows the results of the conductivity measurements performed using liquid Helium as cryogen.

The measured data from sample # 1 (E-glass insulation) can be interpolated using a quadratic function, while all the other data of Fig. 2 can be interpolated using linear functions. The conductivity values of sample # 1 and sample # 2 are close at temperatures below 12 K. The extrapolated value at 4.2 K is 0.1 W/(K-m).

Sample # 3 (epoxy impregnated without insulation) has a higher thermal conductivity, than the insulated samples, with an extrapolated value at 4.2 K of 0.16 W/(K-m).

Samples # 4 and # 5 (ceramic insulation) have a very low thermal conductivity of 0.03 W/(K-m), at 6 and 8 K respectively. Extrapolation to lower temperatures might result in an underestimation of the real conductivity, since the linear interpolating functions have a small, but negative value at zero Kelvin.

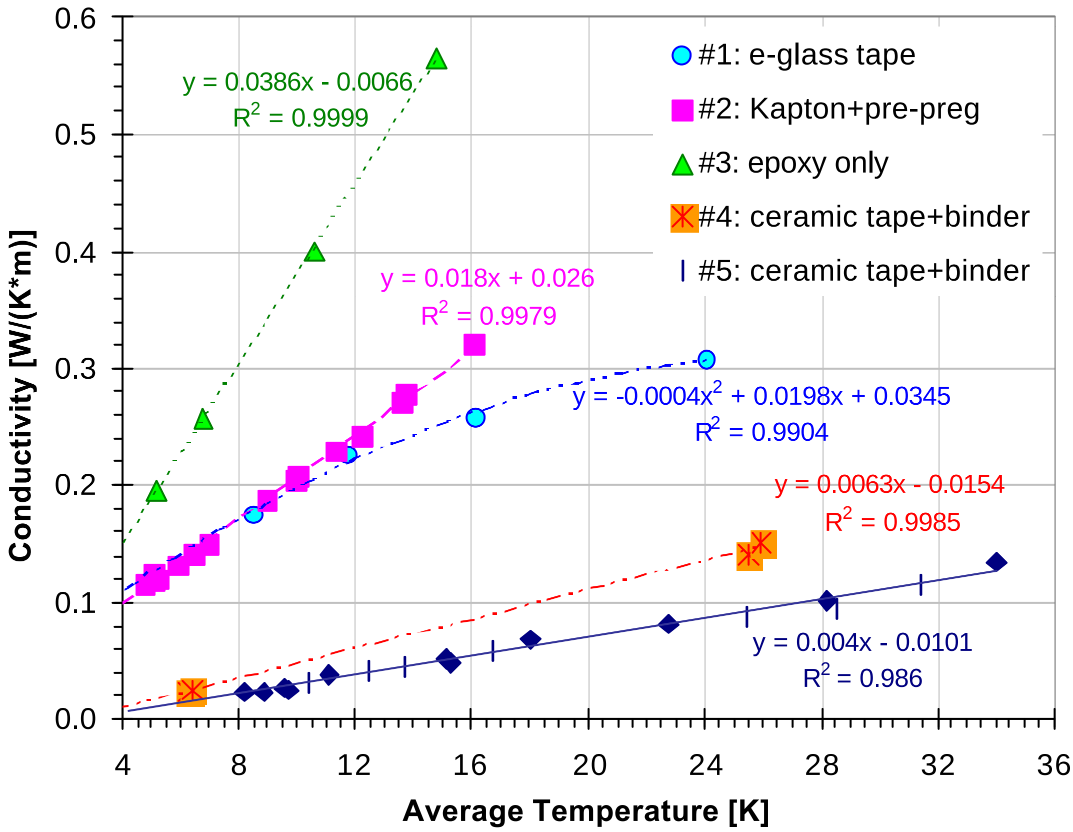

Fig. 2: Results of the conductivity measurements with liquid Helium: experimental data (points) and interpolating functions (dashed lines).

Fig. 3 shows the data of the first three samples, including measurements performed with liquid Nitrogen.

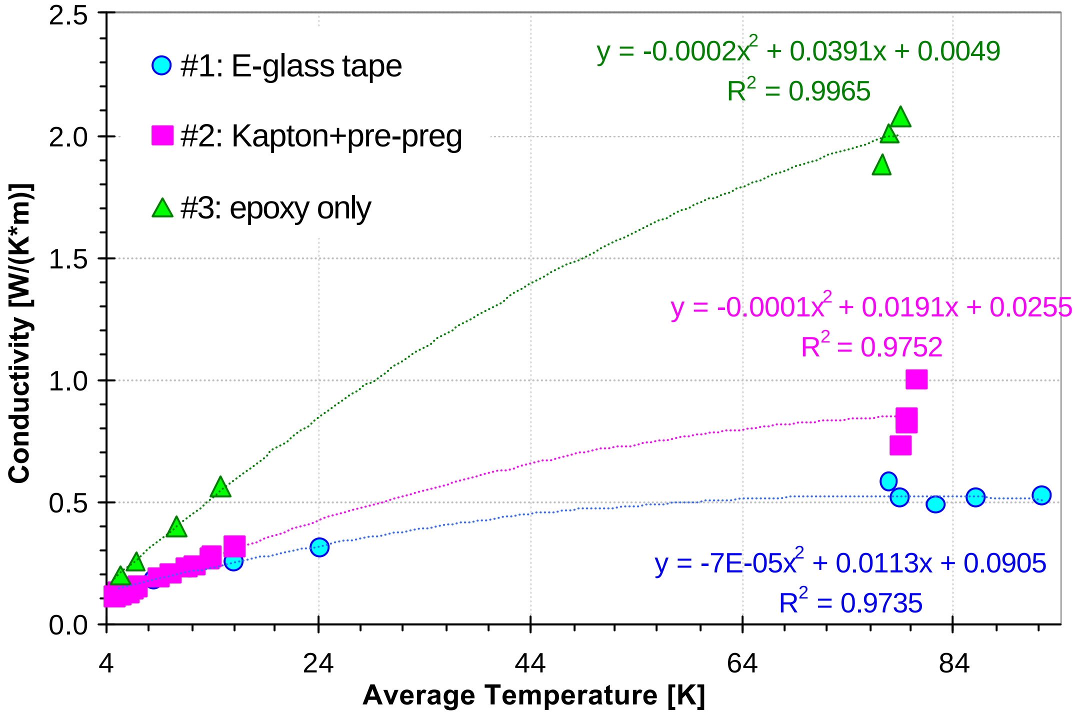

Fig. 3: Results of the conductivity measurements with liquid Nitrogen: experimental data (points) and a quadratic interpolation of the experimental data (dashed lines).

3. Thermal conductivity modeling

The measured data of thermal conductivity of the Nb_3Sn cable stacks were also compared with calculated values from the material properties and the geometrical factors. The comparison can be not only a useful check of the measurement procedure, but can also provide a useful tool to predict the thermal properties in the generic case of a coil with different conductor or insulation characteristics. Therefore, chapter 3 presents:

First, the thermal conductivity of the insulating layer of sample 2, extracted from the measurement data of sample 2 and 3. The results are compared with data from literature to validate the measurement procedure (section 3.1).

Second, the thermal conductivity of the metal part of a cable is considered. Measured data from sample 3 (bare sample) are compared with a detailed model of a Rutherford cable (section 3.2).

Third, the overall thermal conductivity of an impregnated cable stack data, are compared the with calculation results, using a simple model (section 3.3).

3.1 Thermal conductivity of the insulating layer of sample # 2

The thermal conductivity of the insulating layer of sample # 2 (insulated stack) was calculated from the thermal resistance of the sample, subtracting the contribution of the impregnated cable, using the thermal resistance from sample # 3 (bare stack), according to (3):

$$R_{th}\,(\text{ins. layer}) = R_{th}\,(\text{ins. stack}) - R_{th}\,(\text{bare stack}) \quad (1/\mathrm{W}). \tag{3}$$

The resulting thermal conductivity is indicated by the red continuous line in Fig. 4. In the same graph, the thermal conductivity of other insulating materials is also indicated for comparison: G10 (from Cryocomp [9]), Kapton [10], epoxy impregnated fiberglass, IVA-type [11],[12], and the resulting thermal conductivity of 76 μm Kapton and 0.154 mm pre-preg (from above data), indicated by the black dashed line.

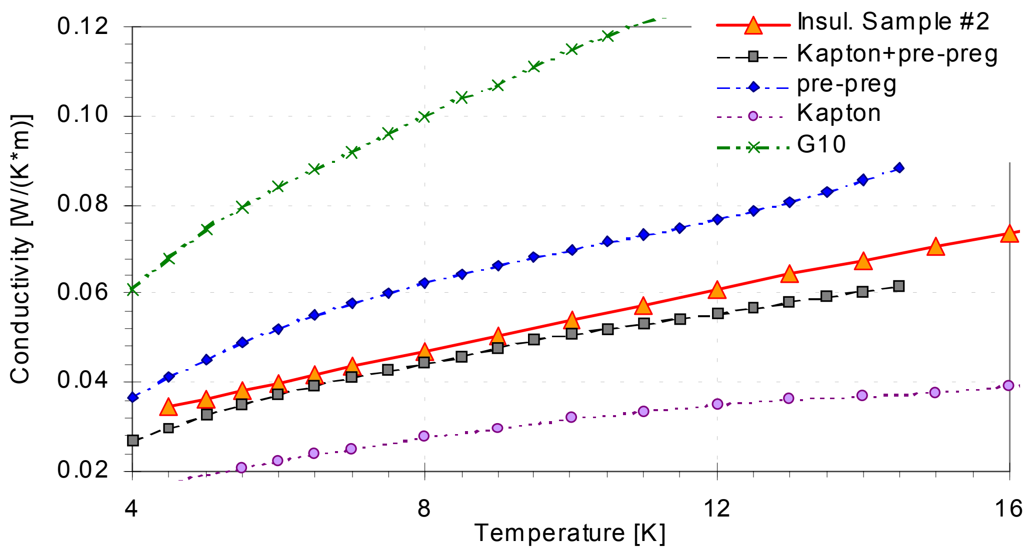

Fig. 4: Thermal conductivity of the insulating material of sample 2, consisting of Kapton and pre-preg tapes, and comparison with other insulations.

The difference between the thermal conductivity of the insulting layer of sample #2 and the conductivity from the data from literature is about 10%. This difference could be due to slightly different pre-preg tapes, in thickness and/or in the epoxy used in the fabrication of the pre-preg tape.

3.2 Thermal conductivity of the bare sample (# 3)

In the following, we present a detailed model of the thermal conductivity of a Rutherford cable in the transverse direction (Fig. 5), that is vertical direction in a Common Coil magnet frame, and azimuthal direction in a cosθ magnet design.

The overall thermal conductivity is determined by the heat conducted in each strand in the transverse direction and the thermal contact resistance between the two layers of strands, and by the heat conducted along the strands due to their transposition.

The results of the calculations are compared with the experimental data of the sample impregnated without insulation.

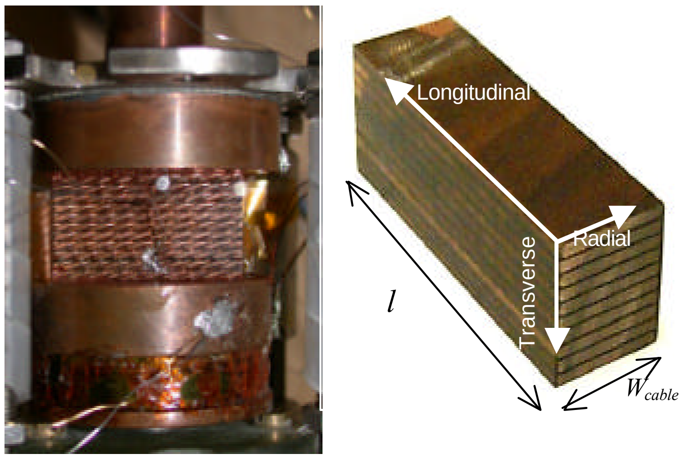

Fig. 5: Sample without insulation (left), and convention for axis labeling, and dimensions; (right).

3.2.a Single strand

To calculate the thermal conductivity in the transverse direction of a Rutherford cable, we first consider the heat flow inside each single strand, without considering the transposition.

In this case (see Fig. 6), the heat flux goes from T_2 to T_1 (with $T_2 > T_1$), mainly through the copper matrix surrounding the superconducting core. In fact, Nb_3Sn, tin, bronze and other materials inside the core, have a much lower conductivity (Fig. 7), even for low RRRs of copper. The RRR of the same conductor was measured for short samples and for the racetrack magnet HFDB02.

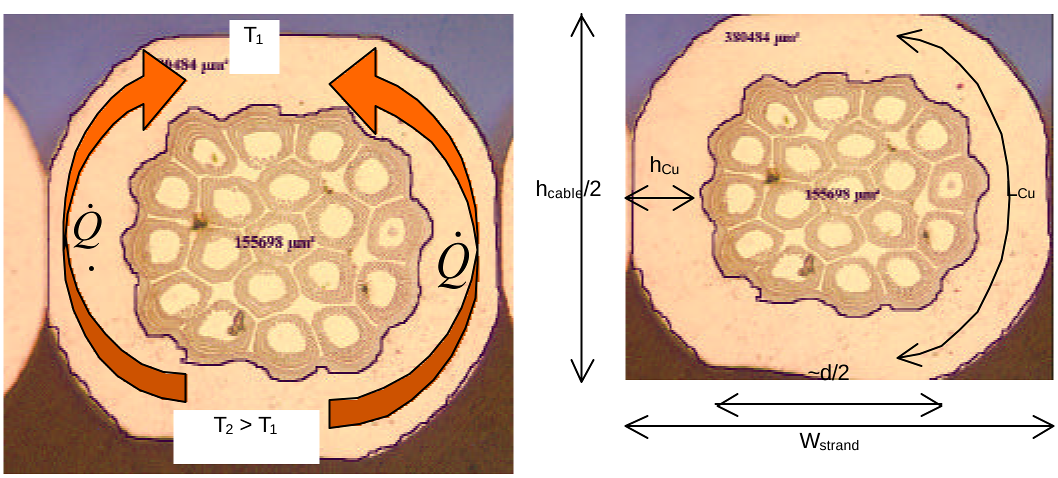

Fig. 6: Picture of a strand in a cable and schematic of heat flow (ITER strand is used just as example), and geometrical parameters determining the axial thermal conductance in a strand.

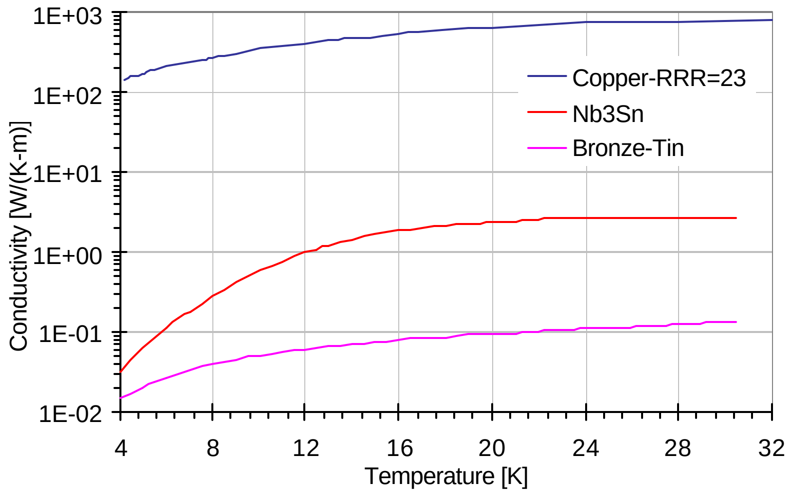

Fig. 7: Conductivity of copper with RRR=23 and B=0 T, from [9]; Nb_3Sn [10], and bronze contained in the superconducting core of a strand, which is contaminated by tin (estimation from Wiedeman-Franz law and measured electrical resistivity)

Hence the strand transverse conductance C_{strand} can be expressed as

$$C_{strand} = 2 \cdot k_{Cu} \cdot \frac{h_{Cu} \cdot l}{L_{Cu}} \quad (\mathrm{W/K}) \tag{4}$$

where the parameters to be used in (4) are given in Table 1.

Symbol	Model parameter	Value
k_{Cu}	Copper thermal conductivity (with RRR = 23, B = 0 T)	see Fig.
h_{Cu}	width of the heat flow path through the copper matrix branches	0.12 mm
l	sample length (~ the length of the strand)	25 mm
$L_{Cu} \sim d$,	length of the heat flow path through the copper matrix branches	0.7 mm
d	strand diameter	0.7 mm
W_{strand}	strand width = $Wcable/(Nstrand/2)$	0.76 mm
$A_{non\text{-}Cu}$	non copper area in the cable cross-section, from Cu/non-Cu = 0.87	8.52 mm^2
N_{strand}	number of strands in the cable	41
h_{cable}	cable thickness	1.3 mm
W_{cable}	cable width	15.14 mm

Table 1: Parameters used to model thermal conductivity in a strand.

Looking at the cable cross-section in Fig. 6, we can approximate $L_{Cu} \sim d$, and h_{Cu} as:

$$h_{Cu} \approx \frac{W_{strand}}{2} - \sqrt{\frac{A_{non-Cu}}{N_{strand} \cdot p}} \quad (\mathrm{m}) \tag{5}$$

Therefore, from $C_{strand} \sim k_{strand} \times W_{strand} \times l \,/(h_{cable}/2)$, we obtain the contribution of each strand to the thermal conductivity in transverse direction, as:

$$k_{strand} = k_{Cu} \cdot \frac{h_{cable}/2}{W_{strand}} \cdot \left(\frac{2 h_{Cu} d}{2 h_{Cu}^{2} + L_{Cu} d} \right) \quad \left(\frac{\mathrm{W}}{\mathrm{K} \cdot \mathrm{m}} \right) \tag{6}$$

3.2.b Contact between strands

The thermal conductivity of a cable in axial direction is reduced drastically when we consider the thermal resistance due to the contact between the two layers of strands. This thermal resistance is difficult to predict, because it depends strongly from the surface characteristics. In particular, for copper, the thermal resistance depends on the oxidation level. This explains why in literature there is a wide range of data values, varying from source to source (Table 2).

Researcher (Reference)	Year	Copper surface	Temp (K)	Applied Force (N)	Conductance (W/K)
Berman	1956		4.2	223	$5.5 \cdot 10^{-3}$
			"	446	$1.02 \cdot 10^{-2}$
			"	670	$1.46 \cdot 10^{-2}$
			"	892	$1.9 \cdot 10^{-2}$
			"	1115	$2.3 \cdot 10^{-2}$
Deutsch	1979		4.2	1004	0.34
Manninen & Zimmerman	1977		4.2	1004	0.34
Nilles and Van Sciver (16)	1988	- Oxidation treatment	5	131	$4 \cdot 10^{-2}$
			290		3.5
		- Clean	4	"	0.1
			290		7
		- N_2 atm.	5	"	0.2
			290		2
Radebaugh et al.	1977		4.2	490	10^{-2}
Salerno et al.	1984-1986		1.6-4.2	22-670	$1 \cdot 10^{-3}$- $2 \cdot 10^{-2}$
Suomi et al.	1968		0.02-0.2	?	10^{-2}

Table 2: Summary of thermal contact literature; from Ref. 11.

"Thermal contact resistance is attributable to several factors, the most notable being that contact between two surfaces is made only at a few discrete locations rather than over the entire surface area. A close examination of even the smoothest surfaces reveals an asperity, which limits the actual area of contact to as few as three discrete locations, irrespective of the dimensions of the sample. This is supported empirically by findings that the thermal conductance of pressed contacts is dependent upon the applied force and not on the area of contact or on the apparent contact pressure. As the applied force is increased, surface deformation of the material occurs. The initial area of contact increases and, as the material deforms further, contact occurs at new locations. The heat flow is constricted in the vicinity of the contact locations because of the narrowness of the effective areas of contact. This constriction is, in large part, responsible for contact resistance. Additionally, the presence of surface films or oxides contributes to the phenomenon. The thickness of these layers adds an additional variable to the conductance. At low temperatures, each oxide layer acts as an additional boundary resistance, and the problem is compounded because of the acoustic mismatch between the layers (Kapitza resistance). Thermal conductance increases asymptotically with increasing applied force. As the applied force increases, the actual area of contact approaches the apparent area. For uncoated samples at liquid helium temperature, it has also been found that thermal conductance is related to the surface finish of the samples.

Experimental data has shown that the thermal conductance of metallic pressed contacts increases according to a simple power law function of temperature, under a given applied force" (from [11]) at LHe temperature.

With increasing temperature from the LHe temperature, the conductance becomes linear with T, and above ~200 K, tends to a temperature independent value. Nilles and Van Sciver [12] performed measurements up to room temperature, of oxide and non-oxide samples, with accurate cleaning procedures, and using N_2 atmosphere (Fig. 8). The non-oxide sample has a conductance that is proportional to the copper conductivity taking into account the geometrical factor (area of the sample and surface roughness) and diving by a factor 25. The oxide sample has a lower conductance at low temperature, and strangely, a higher conductance than the non-oxide sample at room temperature.

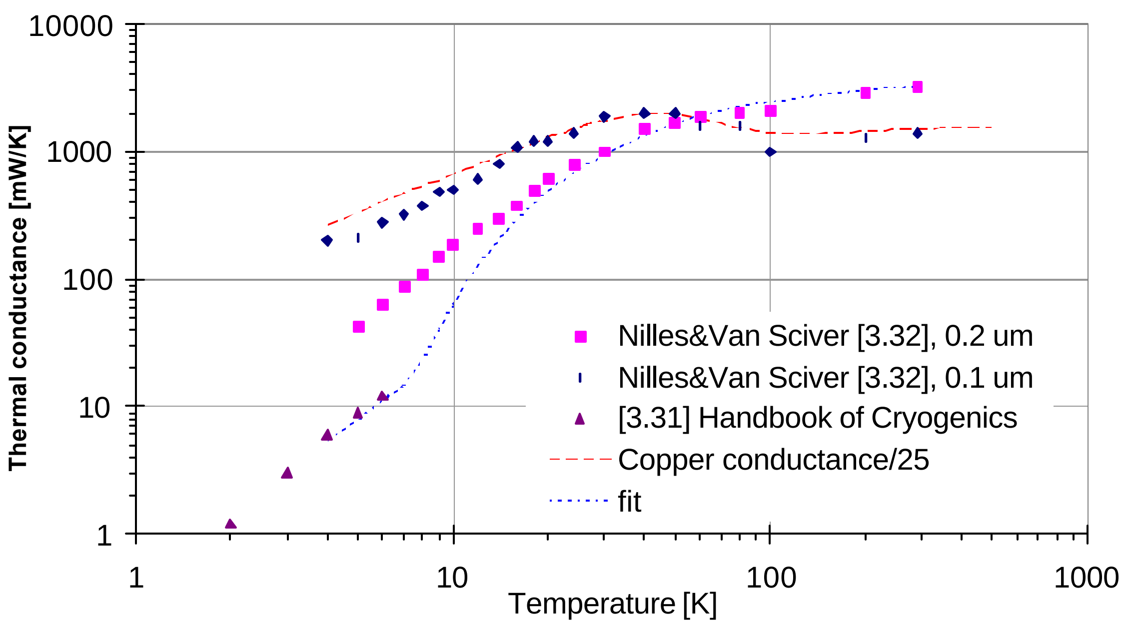

Fig. 8: Thermal conductance of copper sample pairs vs. temperature from different references, and simple models to fit the data.

Since the properties of our samples are not measured, and since there is such a large difference in different samples according to their preparation, a simple model was used to fit the data (dashed line in Fig. 8), in which the conductance follows the power law, at low temperature, and an exponential law up to high temperature. The parameters describing this function are chosen in order to fit the conductivity of the cable sample.

During impregnation of our samples, the pressure was estimated to be about 15 MPa. To obtain the force on the contact area, it is necessary to estimate the actual contact area. If the total area ($A_{tot} = l \cdot W_{cable}$) is reduced by a factor eight, ($A_c = A_{tot}/8$), the resulting force over the contact surface is 735 N. Since it is difficult to measure the exact value of the contact area, this value can be considered a free parameter to fit the experimental data (varying it within a reasonable range [13]).

We considered in the following, the data of copper-to-copper contact with oxide surfaces. The temperature dependence of the contact conductance ($C_{contact}$) is approximated by:

$$\begin{cases} C_{contact}(T) = \boldsymbol{a} \cdot T^n & \text{for } T < T_r = 16\ \mathrm{K} \quad (\mathrm{W/K}) \\ C_{contact}(T) = C_{300} \cdot e^{-1/(b \cdot T)} & \text{for } T > T_r \quad (\mathrm{W/K}) \end{cases} \tag{7}$$

with n = 1.8, $\boldsymbol{a}$ = 0.4 mW/K^{n+1}, C_{300} = 2.7 mW/K, and $\boldsymbol{b}$ is a function of the other parameters, since it is determined by the condition of continuity between the high temperature curve and the low temperature one:

$$\boldsymbol{b} = \left(T_r^n \cdot \ln(\boldsymbol{a} \cdot T_r^n / C_{300})\right)^{-1} = 0.017 \quad (\mathrm{K}^{-1}) \tag{8}$$

The fraction of volume that is not occupied by the metal in a cable stack is filled with epoxy resin. The area occupied by epoxy (A_{epoxy}), in the cable cross-section, can be found by considering the strand area ($A_{met} = N_{strand} \cdot A_{strand}$) and the area of the rectangular cable envelope containing the strands ($A_{cable} = h_{cable} \cdot W_{cable}$). Then $A_{epoxy} = A_{cable} - A_{met}$. Considering a contact area between the strands $W_{cable}/2$ wide, then we obtain an effective thickness of $h_{epoxy} = 2 \cdot A_{epoxy} / W_{cable}$. The resulting contribution of the epoxy to the total conductivity is almost negligible. The formula that describes the conductance of the middle layer (contact conductance plus epoxy conductance) is

$$C_{midplane}(T) = C_{contact}(T) + k_{epoxy} \cdot l \cdot (W_{cable}/2)/h_{epoxy} \quad (\mathrm{W/K}) \tag{9}$$

The total conductance of the cable stack in transverse direction, without considering the transposition of the strands, is given by the series of thermal resistance of the strand layers and of the contact planes:

$$C_{cable} = \left(\frac{2}{C_{strand} \cdot (N_{strand}/2)} + \frac{2}{C_{midplane}} \right)^{-1} \quad (\mathrm{W/K}) \tag{10}$$

where we have considered that in a cable stack, there are two contact planes ("mid-plane") for cable, in average.

The total conductivity of the cable stack in axial direction, without considering the transposition of the strands, is given by:

$$k_{cable} = \left(\frac{1}{k_{strand}} + \cdot \frac{W_{cable} \cdot l}{h_{cable}} \cdot \frac{2}{C_{midplane}} \right)^{-1} \quad \text{(W/m/K)} \tag{11}$$

3.2.c Strand transposition effect on the thermal conductivity

To calculate the effect of the transposition on the transverse thermal conductivity we first have to calculate the thermal conductivity along the strands (k_{long}):

$$k_{long} = \sum_i f_i \cdot k_i \quad \text{(W/m/K)} \tag{12}$$

where $f_i = A_i/A_{Xsection}$ are the fraction of the different components of thermal conductivity k_i, over the cable cross-section area $A_{Xsection}$.

Since the measurements were performed in stationary conditions, let's consider uniform temperatures on planes normal to the axial direction, along which we measured the temperature gradient. This is a good approximation only if we can consider the sample to be homogenous and the heat source to be uniform. In reality, the sample is not homogeneous, and we'll discuss this approximation in the next paragraph. This case is of interest for the study of a quench in a magnet, where the temperature distribution is not uniform, especially close to hot spot.

In the case of uniform temperature on the planes normal to the axial direction, the heat flow involves only the region of the transposition of the strands, at the edge of the cable. This length (L_{transp}) is few millimeters. Since it's difficult to have an exact measure, we used this parameter to fit the experimental data. We have to notice also that the resulting effective thermal conductivity is very sensitive to this value.

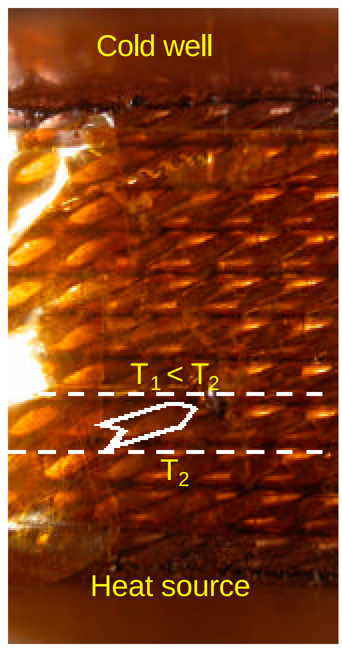

Fig. 9: Bare sample and schematic of the transposition effect for static and homogeneous approximation.

If the sample were half pitch long (l=L_{pitch}), then the contribution to thermal conductance in the axial direction due to the strand transposition (length) would be C_{pitch}:

$$C_{pitch} = k_{long} \frac{A_{X\,section}}{L_{pitch}} = k_{pitch} \frac{L_{trnap} \cdot W_{cable}}{h_{cable}} \quad \text{(W/m/K)} \tag{13}$$

Giving an effective thermal conductivity k_{pitch}

$$k_{pitch} = k_{long} \frac{h_{cable}^{2}}{L_{pitch} \cdot L_{transp}} \qquad \text{(W/(K-m))} \tag{14}$$

Since the measured sample was shorter than half the transposition length, not all the strands were transposed from one layer to the other. The total sample transverse thermal conductivity k_{sample} can be approximated by (14)

$$k_{sample} = k_{cable} + k_{pitch} \cdot l/L_{pitch} \qquad \text{(W/(K-m))} \tag{15}$$

Since not all the strands are transposed (with $l<L_{pitch}$), thermal gradients can establish within the planes normal to the axial direction. In this case, and in case of transient heat diffusion like during a quench, the sample should be considered as inhomogeneous. The transposition length L_{transp} that affects the heat diffusion in (13) can then increase from few millimeters, as in the homogeneous case, to a transposition pitch. In case of $L_{transp}=L_{pitch}$, the contribution of the transposition k_{pitch} to the overall transverse conductivity is small (dashed lines in Fig. 10-13 in the next paragraph).

3.3.d Results of the calculations and comparison with experimental data

There are three main fit parameters, which have a great effect on the sample thermal conductivity:

- α : determining the contact conductance, at LHe temperatures
- C_{300} : determining the contact conductance, at LN temperatures
- L_{transp} : determining the transposition effect.

These parameters are varied together, in order to have k_{sample}, in the homogeneous case, fitting the experimental data. Fig. 10 and Fig. 11 show two fitting curves with different parameters. The continuous line, in this and in the following graphs, represents ksample in the homogeneous case, while the two dashed lines represent ksample in the inhomogeneous case, and with no transposition effect.

In Fig. 10, a low value of contact conductance at low temperature (α = 0.4mW/K$^{2.8}$) was used, together with a short effective transposition length (L_{transp} = 5.3 mm). Fig. 10 shows also the thermal conductivity of the non-homogeneous model, with $L_{transp} = L_{pitch}$ (dashed lines). The conductivity in this case is close to the thermal conductivity of the model that does not consider the transposition effect at all (dotted line).

In Fig. 11, a longer transposition length was used, which requires a higher contact conductance parameter, resulting in a thermal conductivity with non-linear temperature dependence.

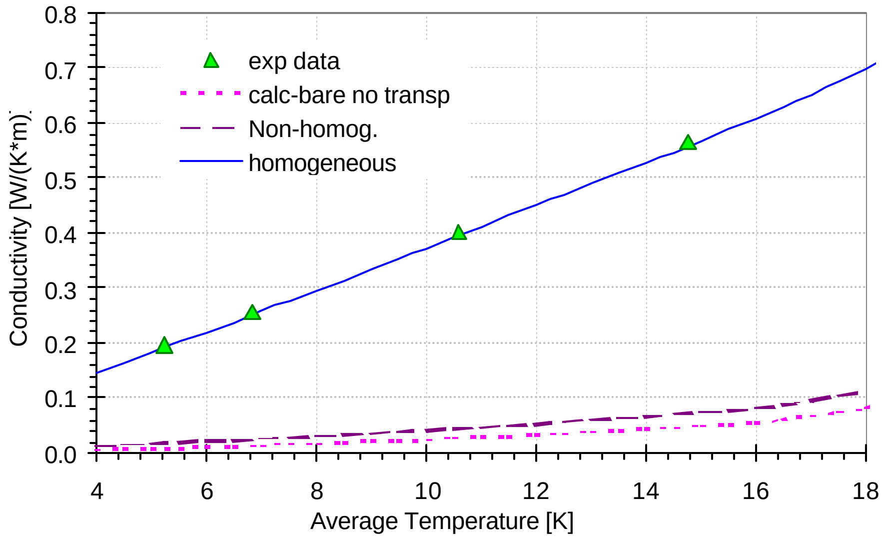

Fig. 10: Sample 3 thermal conductivity data compared to model results, from 4 to 16 K, using a=0.4 mW/K$^{2.8}$, n=1.8, and L_{transp}=5.3 mm.

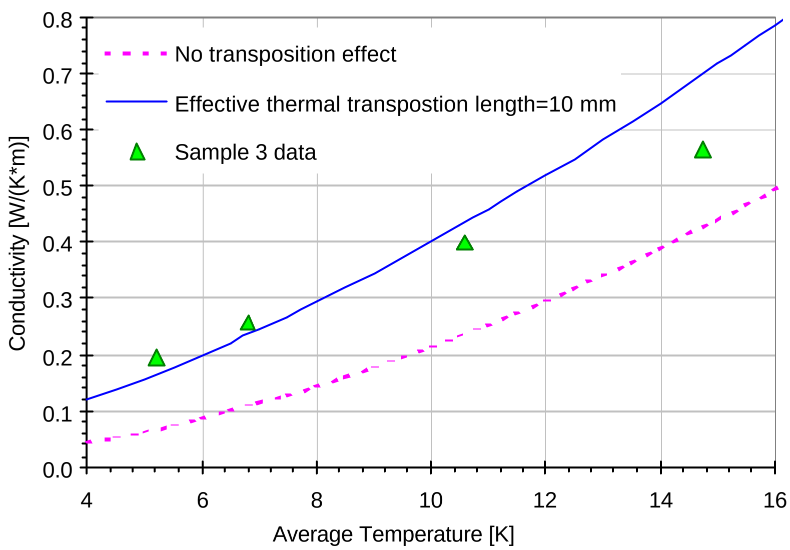

Fig. 11: Sample 3 thermal conductivity data compared to model results, from 4 to 16 K, using a=4 mW/K$^{2.8}$, n=1.8, and L_{transp}=10mm.

The best fit, therefore, is using the fit parameters a = 0.4 mW/K$^{2.8}$, n = 1.8, and L_{transp} = 5.3 mm (as in Fig. 10).

To fit the measured data at LHe and at LN temperatures C_{300} = 4 mW/K was used (Fig. 12).

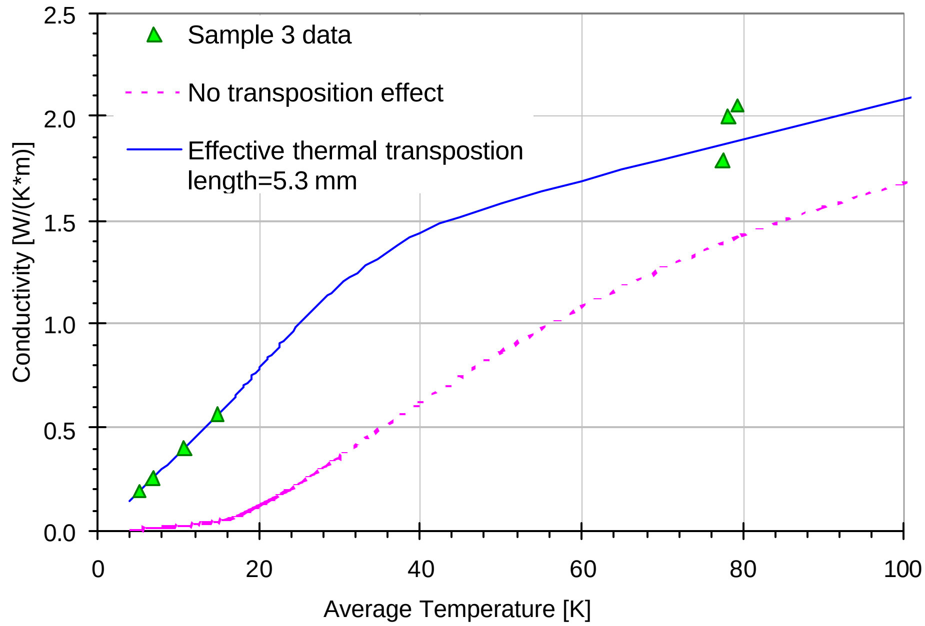

Fig. 12: Sample 3 thermal conductivity data compared to model results, up to LN temperatures, using α=0.4mW/K$^{2.8}$, n=1.8, L_{transp}=5.3 mm and C_{300}=4 mW/K.

Using these values, and with l=L_{pitch}, we obtain the thermal conductivity for a long sample (Fig. 13), which can be useful for thermal analysis of a magnet, such as quench process simulations.

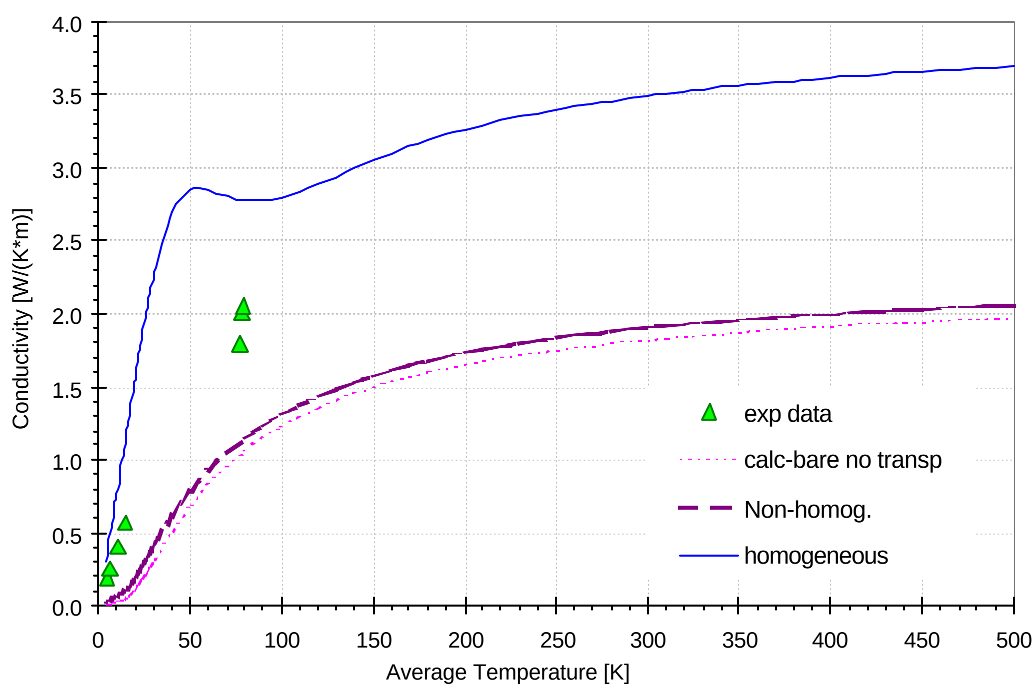

Fig. 13: Sample 3 thermal conductivity data compared to model results using α =0.4 mW/K$^{2.8}$, n=1.8, C_{300}=4 mW/K, and L_{transp}=5.3 mm for a sample half transposition pitch-long or longer. Conductivity extrapolated to 500 K for modeling of the quench.

Fig. 13 shows that longer samples have higher thermal conductivity, due to the contribution to k_{pitch} of all the strands, while in a sample shorter than half the transposition pitch, not all the strands are transposed to the second layer, and therefore cannot contribute to the heat transfer in transverse direction along the strands.

3.3 Overall thermal conductivity of sample # 1 (with e-glass insulation)

The conductivity of the insulated cable stack can also be calculated with a simpler model, where the conductivity of the insulation layer is considered to be like that of pre-preg material (data from [11], [12]), and the conductivity of the bare cable is calculated from the conductivity of the components and their relative surface fraction over the cross section, as a series of thermal resistances. The simple model does not include the contact thermal resistance between strands, or the transposition effect. This simple model is used in the QLASA program to simulate the quench process [14]. The conductance of the sample using QLASA simple model (C_{sample}^{QLASA}) is the sum of the side insulation (C_{insR} that is negligible) and the series of the thermal resistances of the components, as in (15). The height of each layer (h_i) is calculated from the cross-sectional area of the component A_i divided by the cable width: $h_i=A_i/W_{cable}$ (Fig. 14).

$$C_{sample}^{QLASA} = C_{insR} + \frac{W_{cable} \cdot l}{\sum_i h_i/k_i} \quad (\mathrm{W/K}) \tag{16}$$

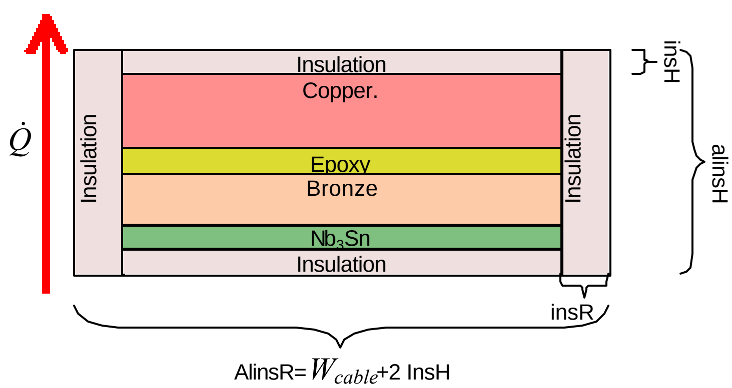

Fig. 14: Schematic of the simple thermal conductivity model for the transverse direction (from QLASA).

Fig. 15 presents a comparison between the simple model conductivity function, and the measured data for sample #1 (E-glass insulation). The two lines of Fig. 15 represent the calculated conductivity, including and not including the epoxy fraction (continuous and dashed lines respectively).

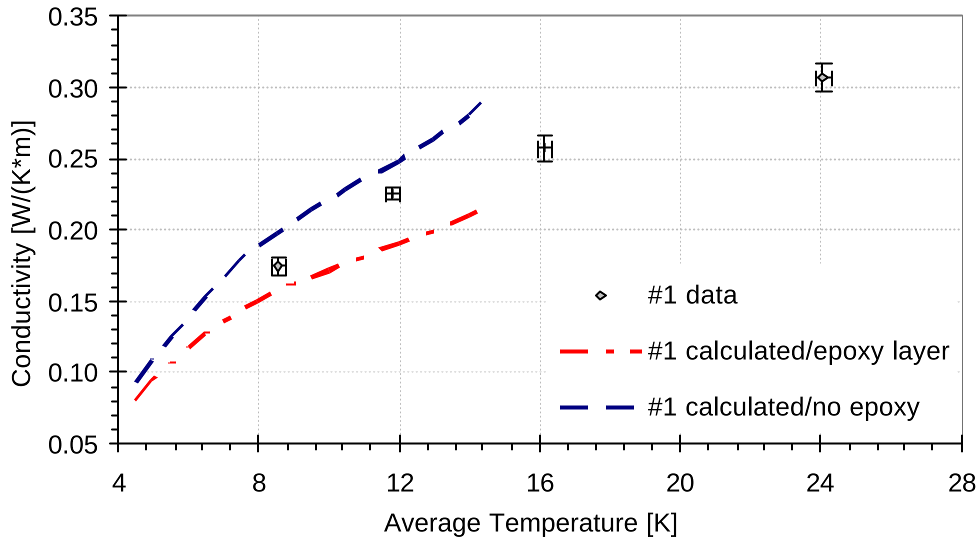

Fig. 15: Comparison of the measured thermal conductivity data with the thermal conductivity calculated from the material properties of the components, for sample #1 (E-glass insulation).

Fig. 15 shows that the thermal conductivity calculated without epoxy, is overestimating the thermal conductivity of sample 1, of a few percent. Including the epoxy, the thermal calculations resulted in an underestimation of the thermal conductivity of sample 1. In fact, the epoxy is included as a continuous layer between the strands while in reality the strands have some contact points. Therefore, the overall thermal conductivity of an insulated cable stack can be estimated, with good approximation, with this simple method, by taking into account only part of the epoxy fraction.

4.0 Summary of thermal conductivity study

The thermal conductivity at cryogenic temperatures of stacks of reacted Nb_3Sn Rutherford cables, with different insulations, and vacuum impregnated with epoxy resin was measured. The different insulation schemes, under study at Fermilab in the frame of Nb_3Sn magnet program, include E-glass, Kapton and pre-preg tapes used for the react-and-wind common coil and racetrack magnets, and ceramic-fiber tape with ceramic binder used for the wind-and react $\cos\theta$ magnets.

Measurements of two samples, one insulated with Kapton and pre-preg, and another without cable insulation, but with otherwise identical characteristics (epoxy-impregnated, same strand parameters etc.) allowed determination of the contribution to the overall coil thermal conductivity of the insulating layer, and of the impregnated cable. The thermal conductivity of the insulating layer was in good agreement with data from literature.

Measured data from the so-called bare (un-insulated) sample were compared with calculations using a detailed model of a Rutherford cable. The analysis included the thermal contact resistance between the two layers of strands of the Rutherford cable, and the effect of the transposition pitch. The contact thermal resistance is difficult to predict, because it depends on the contact surface area and on other insulating materials that can cover the strands, such as oxides and epoxy. For example, the samples fabricated following the procedure of the racetrack magnet included synthetic oil, which was used to prevent sintering of the two layers of strands during reaction. The samples fabricated following the procedure for the cosθ magnet, are believed to have a similar surface contamination, related to the use of a synthetic binder. In fact, the results show that even though the cable had a higher compaction and higher copper content than the cable of the other samples, the overall turn-to turn thermal conductivity is lower. The difference in the conductivity between the cosθ samples can be explained by a difference in the thickness of the coating or in the pressure during preparation.

Even though the transverse conductance of a cable through the contact thermal resistance is small, the transposition of the strands strongly dominates and increases the conductivity of the un-insulated cable, especially at low temperatures.

For an insulated cable stack, the overall thermal conductivity is mainly determined by the turn-to turn insulation. This is the reason why a simple model, approximating the cable stack as a series of thermal resistances of the components, gives results that agree with the measured data, within 10%.

References

[1] V. Zlobin et al. "Conceptual Design Study of Nb_3Sn Low-Beta Quadrupoles for 2nd Generation LHC IRs", ASC02, *IEEE Trans. Appl. Supercond*., June 2003.

[2] Composite Technology Inc., Lafayette, Co

[3] D. R. Chichili et al., "Fabrication and Testing of High Field Dipole Mechanical Model," MT-16, Tallahassee, FL, 1999

[4] G. Ambrosio et al., "Study of Insulating Materials for HFDB-02 Racetrack Magnet using Nb_3Sn and the React-and-Wind Technology," Fermilab TD note, TD-02-08, March 2002

[5] G. Ambrosio, et al., "Fabrication and Test of a Racetrack Magnet Using Pre-Reacted Nb_3Sn Cable," *IEEE Trans. Appl. Supercond*., June 2003.

[6] M. Barzi et al., "Development and Study of Rutherford-type Cables for Accelerators Magnets at Fermilab," *IEEE Trans. Appl. Supercond*., June 2003.

[7] B. Kaspar, G. Ambrosio, P. Bauer, L. Imbasciati, "Contact Resistance Measurement in Nb_3Sn Rutherford Type Cables," Fermilab Technical Division Note, TD-02-39, Nov. 2002

[8] F. Broggi, S. Piuri, L. Rossi, "An Apparatus for Thermal Conductivity Measurements at Cryogenic Temperature on Coil Blocks," INFN/TC-93/01, 1993

[9] Cryocomp v 2.0, Eckels Engineering and Cryodata Inc., normal to cloth G10 properties

[10] Measurements at CERN, private communication

[11] F. Rondeaux, P. Bredy, J.M. Rey, CEA Saclay, "Thermal Conductivity Measurements of Epoxy Systems at Low Temperature," Advances in Cryogenic Engineering Materials, Vol. 48A, pg 197

[12] M. Damasceni, L. Rossi, S. Visona, "Measurements at cryogenic Temperature of the Thermal Conductivity of the ground Insulation of a Model of the ATLAS BT coils," tech. Rep. LASA/ATLAS/510 (1998)

[13] MATPRO, electronic library of QLASA; copper conductivity calculated by F.M. Ametrano, F. Broggi

[14] MATPRO, electronic library of QLASA; Nb_3Sn thermal conductivity from Brechna p. 424

[15] L.J. Salerno and P. Kittel, *Handbook of cryogenics*, Chapter 3, from p. 167

[16] M.J. Nilles and S.W. Van Sciver, "Effects of Oxidation and Roughness on Cu Contact Resistance from 4 K to 290 K," Adv. in Cryog. Eng. Mat., Vol 34

[17] J-M. Depond, D. Leroy, L. Oberli, "Superconducting Cable Topology," Internal Note 97-09, LHC-MMS

[18] M. Canali, L. Rossi, "DYNQUE: a Computer Code for Quench Simulation in Adiabatic Multicoil Superconducting Solenoids," INFN/TC-93/06, 1993